Absorbing and Connecting Boundary Conditions for the TLM Method

Zhizhang Chen, *Member, IEEE,* Michel M. Ney, *Senior Member, IEEE,* and Wolfgang J. R. Hoefer, *Fellow, IEEE*

***Abstract*—Absorbing and connecting boundary conditions are implemented for the transmission-line matrix (TLM) method. The approach is based on an equivalence previously established between the finite-difference–time-domain (FD–TD) method and the TLM method. Boundary conditions presently used for the FD–TD algorithm can be transformed into conditions that can be interfaced with two-and three-dimensional (2D and 3D) TLM schemes. Additional conditions are introduced for 3D-TLM symmetrical condensed node simulations to suppress instabilities caused by spurious modes, inherent to the model, and which are amplified by absorbing boundaries. Numerical results and the comparison with other methods show the good performance of the proposed algorithms.**

I. Introduction

Since its introduction by Johns [1], the transmission-line matrix (TLM) method has been used extensively to solve electromagnetic problems that pertain to a wide variety of applications [2], [3]. The major advantages of this method are the simplicity and flexibility of its basic algorithm, from which vectorial Maxwell's equations are transformed into a simple numerical model of wave propagation.

Like finite-difference–time-domain (FD–TD) and finite element methods, recent publications have shown that TLM can be used for open problems for which various techniques have been used to limit the computational domain. For instance, Eswarappa *et al.* [4] used Johns' matrix techniques to simulate matched loads in rectangular waveguides for the dominant modes. Regarding scattering problems, Simons and Bridges [5], [6] derived 2D-TLM absorbing boundaries, and Saguet [7] proposed matched load simulation based on Taylor's series expansion technique for 2D-TLM waveguide problem simulations. More recently, Morente *et al.* [8] investigated TLM absorbing boundaries based on a one-way equation technique for three-dimensional problems. If relatively little work has been reported on absorbing boundaries for TLM, many approaches to implement absorbing boundaries for the FD–TD method have been reported in the literature. Among algorithms that have shown good performance are Liao *et al.*'s [9], Higdon's [10], and Lindman's [11] absorbing boundary conditions. These FD–TD conditions have been studied by Blaschak and Kriegsmann [12], Fang [13], Moore *et al.* [14], and Railton and Daniel [15].

Manuscript submitted September 10, 1992; revised January 28, 1993.

Z. Chen and M. M. Ney are with the Laboratory for Electromagnetics and Microwaves, Department of Electrical Engineering, University of Ottawa, Ontario, Canada.

W. J. R. Hoefer is with the Department of Electrical Engineering, University of Victoria, British Columbia, Canada.

IEEE Log Number 9212724.

In addition to proper absorbing boundaries, it is necessary for scattering problems to introduce connecting boundaries [16], [17]. These are artificial boundaries that separate regions within which scattered fields only prevail from the ones where the total field (incident and scattered fields) exists. Their purpose is to avoid incident plane waves to impinge on absorbing walls for which they exhibit poor performance. A two-dimensional algorithm was proposed for TLM simulations [6] and is based on the equivalence principle.

Since each TLM scheme is equivalent to a FD–TD formulation as presented in [18], absorbing and connecting conditions developed for the FD–TD method can be transimplemented into TLM simulations. In this paper, Higdon's absorbing conditions, Taylor's expansion algorithm, and connecting boundary conditions for the FD–TD method are modified and implemented into the 2D-TLM and extended to 3D-TLM simulations.

II. Absorbing Boundary Conditions

An absorbing boundary scheme that uses a dissipation region that gradually damps waves striking the boundary was reported [4]. However, to obtain substantial absorption over a wide range of wave incident angles and frequencies, dissipation must occur within a region that extends over several wavelengths of the lowest frequency component. Two other techniques to generate absorbing boundaries for 2D problems were presented. The first method used a technique to adjust the local reflection coefficient at every point on absorbing walls and simulation time step. Evaluation of that coefficient was based on the wave local incident angle, predicted by a special field extrapolation routine [5]. Some difficulties associated with deriving a good algorithm for predicting accurate incident angles for general cases were reported. The second technique directly applied Higdon's absorbing conditions for the FD–TD method to the 2D-TLM simulations [6]. However, this approach does not give satisfactory results with the 3D-TLM symmetrical condensed node, due to rapid generation of unstable solutions. Very recently, an approach based on a one-way equation and a technique based on a discrete form of the wave equation were proposed [8]. If satisfactory results were obtained for 2D problems, instabilities were reported for 3D cases.

A. Taylor's Expansions

Consider a spatial domain $\Omega = (x, y, z), x < 0$, with an absorbing boundary placed at $x = 0$. Then, by assuming

that the wave propagates along the positive X direction, one can have $x - ct = \text{const}$, or $\Delta x/\Delta t = c$ (Δx and Δt are the space and time increments, respectively), for the wave function $U = U(x, y, z, t)$. Then, $U = U(x, y, z, t)$ can be approximated by a Taylor's series (Taylor's expansion) along the plane of $x - ct = \text{const}$. As a result, one has

$$U(0, y, z, t) \approx U(0 - \Delta x, y, z, t - \Delta t) + \sum_{i=1}^{P} \frac{1}{i!} \frac{\partial^i U(0 - \Delta x, y, z, t - \Delta t)}{\partial x^i} \cdot (\Delta x)^i, \quad (1)$$

where integer P is the order of expansion.

By replacing $U(x, y, z, t)$ with ${}_nU(i_x, i_y, i_z)$ [$= U(i_x \Delta x, i_y \Delta y, i_z \Delta z, n \Delta t)$] and the differential with backward difference, one can easily have the updated value of the wave function at the boundary:

$${}_nU(0, i_y, i_z) \approx {}_{n-1}U(0 - 1, i_y, i_z) + \sum_{i=1}^{P} \frac{1}{i!} \frac{\nabla^i_{n-1} U(0 - 1, i_y, i_z)}{(\Delta x)^i} (\Delta x)^i. \quad (2)$$

The backward differences are computable since they are evaluated inside the spatial domain Ω. Thus, the preceding condition is suitable for an absorbing boundary and can be rewritten as

$${}_nU(0, i_y, i_z) \approx \sum_{i=1}^{P} a_{i,i}\, {}_{n-i}U(0 - i, i_y, i_z) \quad (3)$$

or

$$\left(\sum_{i=0}^{P} a_{i,i} D_x^{-i} K^{-i} \right) {}_nU(0, i_y, i_z) = 0, \qquad a_{0,0} = -1, l \quad (4)$$

where $a_{i,i}, i = 0, \cdots, P$, is the expansion coefficient that can be obtained by expanding (2) (see Table I), ${}_nU(0, i_y, i_z)$ is the updated value of the wave function at the absorbing boundary, and D_x^{-i} and K^{-i} are the space and time-shifting operators defined as follows:

$$D_x^{-i}\, {}_nU(i_x, i_y, i_z) = {}_nU(i_x - i, i_y, i_z) \quad (5)$$

$$K^{-i}\, {}_nU(i_x, i_y, i_z) = {}_{n-i}U(i_x, i_y, i_z). \quad (6)$$

The quality of the preceding absorbing boundary can be evaluated by examining the reflection coefficients of the boundary [14]. Fig. 1 shows the reflection coefficients of Taylor's expansions at $\Delta x/\lambda = \Delta l/\lambda = 0.025$ for a medium of $\mu_r = 1$ and $\varepsilon_r = 2$.

B. Higdon's Absorbing Boundary Conditions

Again, consider a spatial domain $\Omega = (x, y, z), x < 0$, with an absorbing boundary placed at $x = 0$. Higdon [10] proposed the following form of absorbing conditions:

$$\prod_{i=1}^{P} \left(\frac{\partial}{\partial x} + \frac{\cos(\theta_i)}{c} \frac{\partial}{\partial t} \right) U(x, y, z, t) = 0, \quad (7)$$

where $\theta_i, i = 1, \cdots, P$, is the incident angle at which the wave is supposed to be exactly absorbed. The preceding condition has been claimed to provide a general and optimal representation among those absorbing boundary conditions based on a systematic rational approximation to the portion of the dispersion relation. The θ_i can be chosen the same as those obtained in [19] with the different optimization criteria for wide-angle absorption. However, the choice of θ_i, in general, depends on the configuration of the problem to have the best absorption. For example, θ_i may be chosen to take advantage of *a priori* information about the directions to which particular waves approach the boundary.

Now, taking difference approximations for both $\partial/\partial x$ and $\partial/\partial t$, (7) becomes

$$\prod_{i=1}^{P} \left[\left(\frac{1 - D_x^{-1}}{\Delta x} \right) \frac{1 + K^{-1}}{2} + \frac{\cos(\theta_i)}{c} \left(\frac{1 - K^{-1}}{\Delta t} \right) \cdot \left(\frac{1 + D_x^{-1}}{2} \right) \right] {}_nU(0, i_y, i_z) = 0. \quad (8)$$

TABLE I
COEFFICIENTS FOR DIFFERENT ORDER OF TAYLOR'S EXPANSION

Order of the Absorbing Boundary P	Coefficients
1	$a_{11} = 1.0000$
2	$a_{11} = 2.0000$ $a_{22} = -1.0000$
3	$a_{11} = 2.5000$ $a_{22} = -2.0000$ $a_{33} = 0.5000$
4	$a_{11} = 2.6667$ $a_{22} = -2.5000$ $a_{33} = 1.0000$ $a_{44} = -0.1667$
5	$a_{11} = 2.7083$ $a_{22} = -2.6667$ $a_{33} = 1.2500$ $a_{44} = -0.3333$ $a_{55} = 0.0417$

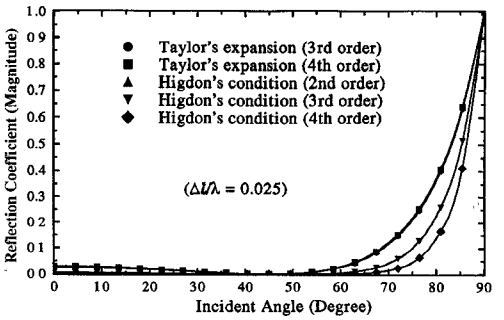

Fig. 1. Reflection coefficients of Taylor's Expansion and Higdon's conditions.

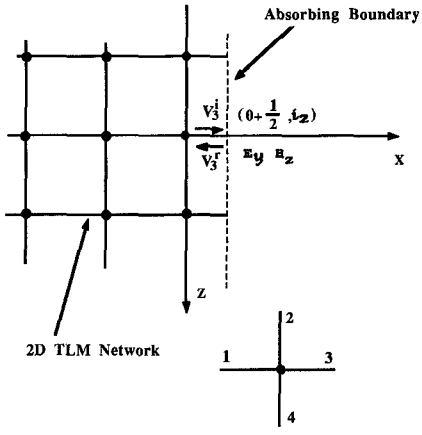

Fig. 2. 2D-TLM network with absorbing boundary.

After some mathematical manipulations, (8) can be expressed as

$$ {}_nU(0,i_y,i_z) = \sum_{i1=0}^{P}\sum_{i2=0}^{P} a_{i1,i2}\, {}_{n-i2}U(0-i1,i_y,i_z), \qquad a_{0,0}=0 \tag{9}$$

or

$$ \sum_{i1=0}^{P}\sum_{i2=0}^{P} a_{i1,i2}\, D_x^{-i1}K^{-i2}\, {}_nU(0,i_y,i_z), \qquad a_{0,0}=-1\,, \tag{10}$$

where $a_{i1,i2}$ depends only on the types of absorbing boundary conditions used, and can be obtained by expanding (8). ${}_nU(0,i_y,i_z)$ is the updated value of the wave function at the absorbing boundary.

The reflection coefficients of Higdon's absorbing conditions can be evaluated similarly to that for Taylor's expansion. Comparisons for different orders of absorbing conditions are shown in Fig. 1. In fact, both Higdon's conditions and Taylor's expansion can be generally expressed mathematically by (10). That is, the wave at the boundary is predicted by a linear function of waves inside and on the boundary at the previous time steps. Whereas the different sets of constants $a_{i1,i2}$, as a consequence of different ways of approximation, have led to different types of absorbing conditions, they are essentially related to extrapolation techniques. Higdon's conditions and Taylor's expansion can be considered as a wave expansion (or extrapolation) along plane $x-ct=\text{const}$. Other approaches used the multidimensional expansion, in which tangential field components are also employed to evaluate the unknown, for instance, Lindman's conditions [11].

III. Implementation of Absorbing Boundary Conditions in TLM Simulations

Consider a spatial domain $\Omega = (x,y,z), x \le (1/2)\,\Delta x$ (Fig. 2), in which a TLM mesh is positioned and an absorbing boundary is placed at $x = (1/2)\,\Delta x$. The objective is to find the impulse reflected by the boundary while maintaining minimum, global reflections.

As shown in [18], the impulse in the TLM mesh is actually equivalent to the linear combination of electric and magnetic field components. For example, in Fig. 2,

$$\begin{aligned} {}_{n+\frac{1}{2}}V_3^r\left(0+\frac{1}{2},i_y,i_z\right) &= {}_{n+\frac{1}{2}}V_y\left(0+\frac{1}{2},i_y,i_z\right) \\ &\quad + Z_0\, {}_{n+\frac{1}{2}}I_x\left(0+\frac{1}{2},i_y,i_z\right) \\ &\equiv {}_{n+\frac{1}{2}}E_y\left(0+\frac{1}{2},i_y,i_z\right) \\ &\quad - Z_0\, {}_{n+\frac{1}{2}}H_z\left(0+\frac{1}{2},i_y,i_z\right). \end{aligned} \tag{11}$$

Since both E_y and H_z satisfy the wave equation, the absorbing boundary conditions can be applied to either of them or to the linear combination of them [e.g., ${}_{n+(1/2)}V^r(0+1/2,i_y,i_z)$ in this case] such that waves propagate through the boundary with minimum reflections. In consequence, the absorbing boundary conditions presented can be generally and directly applied to impulses traveling in the TLM network. More specifically, in the formulations of the absorbing condition with Taylor's expansion and Higdon's conditions shown earlier, wave function U can be considered as impulses V on the link lines of the TLM nodes, including those located at the absorbing boundary. This results in the formulations of absorbing boundary conditions for the TLM simulations.

A. Absorbing Boundaries for 2D-TLM Node

Consider the 2D-TLM shunt node model as shown in Fig. 2, in which an absorbing boundary is placed at $x = 0+(1/2)\,\Delta x$ (halfway between nodes). The impulse ${}_{n+(1/2)}V_3^r(0+1/2,i_z)$,reflected by the absorbing boundary and to be injected back to the TLM network, can be found easily according to (10) as

$$\begin{aligned} {}_{n+\frac{1}{2}}V_3^r\left(0+\frac{1}{2},i_z\right) &= \sum_{i1=0}^{P}\sum_{i2=0}^{P} a_{i1,i2} \\ &\quad \cdot {}_{n+\frac{1}{2}-i2}V_3^r\left(0+\frac{1}{2}-i1,i_z\right) = 0, \\ a_{0,0} &= 0 \end{aligned} \tag{12}$$

or

$$\begin{aligned} \sum_{i1=0}^{P}\sum_{i2=0}^{P} a_{i1,i2}\, D_x^{-i1}K^{-i2}\, {}_{n+\frac{1}{2}}V_3^r\left(0+\frac{1}{2},i_z\right) &= 0, \\ a_{0,0} &= -1\,, \end{aligned} \tag{13}$$

where $a_{i1,i2}$ pertain to different types of absorbing boundaries used.

For the 2D-TLM series node, a similar condition can be developed.

B. Absorbing Boundaries for 3D-TLM Expanded Node and Asymmetrical Condensed Node

Since the 3D expanded node model and the 3D asymmetrical condensed model are constructed from the 2D-TLM shunt

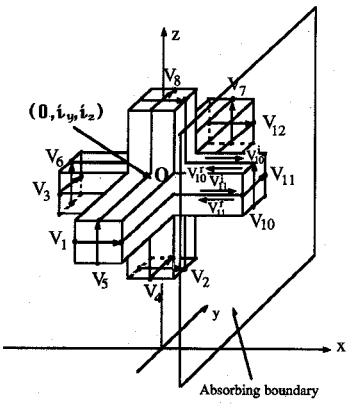

Fig. 3. 3D-TLM symmetrical condensed node with absorbing boundary.

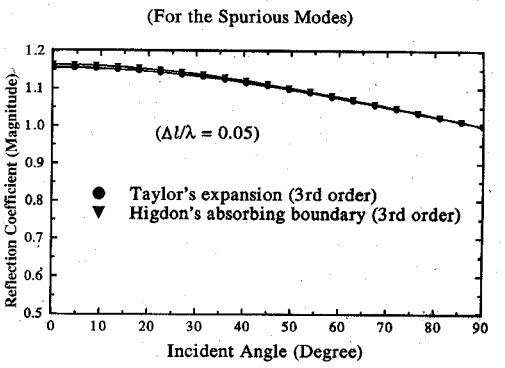

Fig. 4. Reflection coefficients of absorbing boundaries for spurious modes.

and series node models, the corresponding absorbing boundary conditions can be established in a way similar to that described for the 2D-TLM simulation. More specifically, the impulse reflected by the boundaries and to be injected back into the TLM network can also be found by (13). The only difference resides in the assignment of the superscripts and subscripts for V since their numbers depend on which link lines are connected to the boundaries.

C. Absorbing Boundaries for 3D-TLM Symmetrical Condensed Node

For the 3D-TLM symmetrical condensed node (SCN), the absorbing boundaries are still valid except that K^{-i1} must be replaced by K^{-2i1}. This modification is due to the slow-wave property of the 3D-TLM SCN model: The scattered impulse on the link line of a node, resulting from an incident impulse with the same polarization on the link line at the other side of the node, only appears after two time steps $2\Delta t$. Consequently, the modified condition can be expressed as (referring to Fig. 3)

$$\sum_{i1=0}^{P}\sum_{i2=0}^{P} a_{i1,i2}\, D_x^{-i1} K^{-2i2}{}_{n+\frac{1}{2}} V^r_{10\,\text{or}\,11}\left(0+\frac{1}{2}, i_z\right) = 0, \qquad a_{0,0} = -1\,. \tag{14}$$

However, despite the preceding modifications, simulations have shown that the uncontrollable instability may occur when the absorbing conditions are implemented directly into the 3D SCN model. The main reason is that spurious modes can propagate in the 3D-TLM SCN model and, although they may have relatively small magnitude, can be amplified by the absorbing boundary conditions.

1) Spurious Modes and Their Effects at Absorbing Boundaries: Nielsen [20] has shown that, due to periodic spatial sampling and symmetry, spurious modes exist in the 3D-TLM symmetrical condensed node model. their existence can be explained by the fact that the TLM model cannot correctly simulate high spatial-frequency components due to the finite discretization in space. Therefore, the spurious modes will be produced to substitute the high spatial-frequency physical components wherever required.

The existence of the spurious modes can be described quantitively as follows: suppose a physical mode, which is expressed by (15), propagating in the 3D-TLM SCN network

$${}_nU(i_x,i_y,i_z) = e^{j(\omega n\,\Delta t - k_x i_x\,\Delta_x + k_y i_y\,\Delta_y + k_z i_z\,\Delta_z)} \tag{15}$$

with propagation constants k_x, k_y, and k_z and temporal frequency ω.

Then, the forward-propagating spurious mode, expressed by (16), and backward-propagating spurious mode, expressed by (17), can propagate, both with the same temporal frequency ω and propagation constants $\bar{k}_x = \frac{\pi}{\Delta x} + k_x, \bar{k}_y = \frac{\pi}{\Delta y} + k_y$, and $\bar{k}_z = \frac{\pi}{\Delta z} + k_z$.

$${}_nU(i_x,i_y,i_z) = e^{j(\omega n\,\Delta t - \bar{k}_x i_x\,\Delta x + \bar{k}_y i_y\,\Delta y + \bar{k}_z i_z\,\Delta z)} \tag{16}$$

$${}_nU(i_x,i_y,i_z) = e^{j(\omega n\,\Delta t + \bar{k}_x i_x\,\Delta x + \bar{k}_y i_y\,\Delta y + \bar{k}_z i_z\,\Delta z)} \tag{17}$$

These spurious waves are represented by spheres centered at (π,π,π) in a three-dimensional dispersion diagram (see [20]), and their propagation constants $\bar{k}_x, \bar{k}_y$, and $\bar{k}_z$ have large values because Δx, Δy, and Δz are small. Thus, spurious modes are nonphysical entities with high spatial-frequency components. They are generated by spurious excitations, geometries with discontinuities, and can even propagate with low temporal frequency content. When absorbing boundary conditions are applied, spurious modes can be amplified at the boundary. The reflection coefficients for the spurious modes have been computed and are shown in Fig. 4. As can be seen, the reflection coefficients are larger than one, leading to instability.

2) The Modified Absorbing Boundary Conditions for 3D-TLM Symmetrical Condensed Node: To reduce the effects of spurious modes at absorbing boundaries, additional conditions may be introduced. Suppose that there exist a physical mode, expressed by (15), and its spurious mode, expressed by (16). The phase shift between two neighboring nodes along $x =$ const for the physical mode is $k_x\,\Delta x$, whereas for the spurious mode it is $\bar{k}_x\,\Delta x = \pi + k_x\,\Delta x$, which corresponds to a change of polarity in addition to the phase shift of the physical mode. Therefore, if an absorbing boundary condition exists for the physical modes as indicated by (14),

$$\sum_{i1=0}^{P}\sum_{i2=0}^{P} a_{i1,i2}\, D_x^{-i1} K^{-2i2}{}_{n+\frac{1}{2}} V^r_{10\,\text{or}\,11}\left(0+\frac{1}{2}, i_y, i_z\right) = 0, \qquad a_{0,0} = -1\,, \tag{18}$$

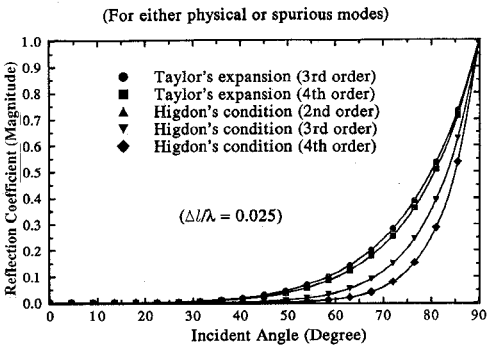

Fig. 5. Reflection coefficients of modified absorbing boundaries.

then, the condition

$$\sum_{i1=0}^{P}\sum_{i2=0}^{P}(-1)^{i1}a_{i1,i2}\,D_x^{-i1}K^{-2i2} \cdot {}_{n+\frac{1}{2}}V^r_{10\text{ or }11}\left(0+\frac{1}{2},i_y,i_z\right)=0,$$
$$a_{0,0}=-1, \tag{19}$$

should absorb the forward-propagating spurious mode.

By combining the preceding two conditions, one can easily obtain the condition that can absorb both the physical and spurious modes:

$$\left(\sum_{i1=0}^{P}\sum_{i2=0}^{P}a_{i1,i2}\,D_x^{-i1}K^{-2i2}\right)\cdot\left(\sum_{i1=0}^{P}\sum_{i2=0}^{P}(-1)^{i1}a_{i1,i2}\,D_x^{-i1}K^{-2i2}\right)\cdot {}_{n+\frac{1}{2}}V^r_{10\text{ or }11}\left(0+\frac{1}{2},i_y,i_z\right)=0. \tag{20}$$

Fig. 5 shows the reflection coefficients using the preceding absorbing condition for physical and spurious modes under the assumption that $k_x = k\cos\theta$, where θ is the incident angle to the absorbing boundaries. Compared with Fig. 1, good absorption still can be observed for the modified algorithm.

IV. Connecting Boundary Conditions for TLM Simulations

Absorbing boundary conditions have been found to perform poorly with plane waves [11], which may be explained by the fact that they do not satisfy radiation conditions. Consequently, it is essential to separate scattered fields from the total field in regions adjacent to absorbing boundaries. This is achieved by introducing connecting boundaries as illustrated by Fig. 6. Note that although there are other ways to deal with scattering problems [13], the technique presented here may avoid numerical noise in certain situations [16], [17]. In addition to some pioneering work presented by Simons and Bridges [6] for two-dimensional scattering problems, a more concise and general formulation for connecting conditions is proposed here and extended to the 3D case. The approach is based on the equivalence between the TLM method and the new FD–TD formulation described in [18].

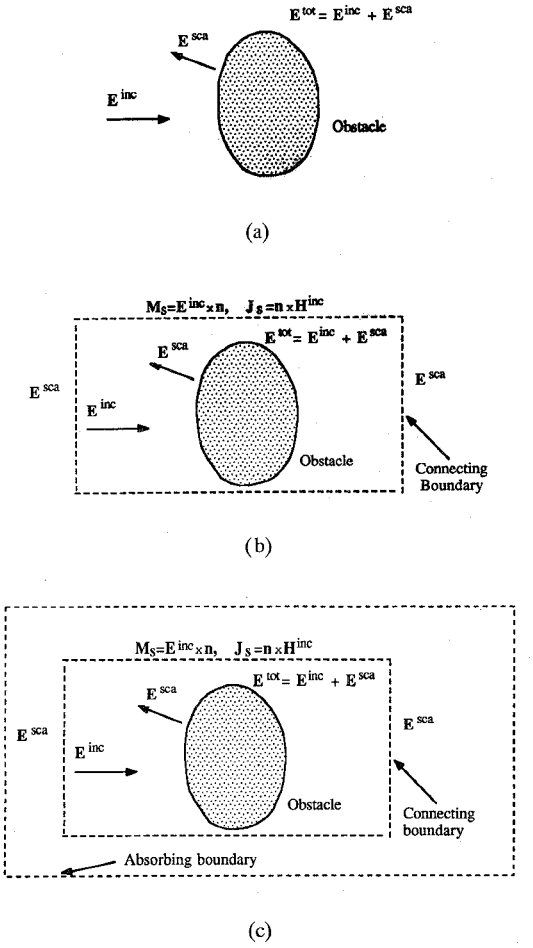

Fig. 6. Obstacle illuminated by electromagnetic wave: (a) original problem; (b) equivalent problem; and (c) equivalent problem with absorbing boundaries.

Consider the electromagnetic scattering by an object in Fig. 6(a). For linear media, the total field can be decomposed into incident and scattered fields. That is,

$$\mathbf{E}^{\text{tot}} = \mathbf{E}^{\text{inc}} + \mathbf{E}^{\text{sca}} \tag{21}$$

$$\mathbf{H}^{\text{tot}} = \mathbf{H}^{\text{inc}} + \mathbf{H}^{\text{sca}} \tag{22}$$

where the incident fields $\mathbf{E}^{\text{inc}}$ and $\mathbf{H}^{\text{inc}}$ are defined as fields that exist in the absence of the scatterers.

According to the equivalence principle [22], solving the problem in Fig. 6(a) can be substituted to solving the problem of Fig. 6(b) or 6(c) under the condition that a magnetic current source

$$\mathbf{M}_s = \mathbf{E}^{\text{inc}} \times \mathbf{n} \tag{23}$$

and an electric current source

$$\mathbf{J}_s = \mathbf{n} \times \mathbf{H}^{\text{inc}} \tag{24}$$

exist on the connecting surface, where $\mathbf{n}$ is the normal unit vector of the connecting surface pointing inward.

Now, suppose that a connecting boundary is placed between two regions filled with a TLM network, as shown in Fig. 7.

Writing

$$\mathbf{M}_s = M_y\mathbf{a}_y + M_z\mathbf{a}_z \tag{25}$$

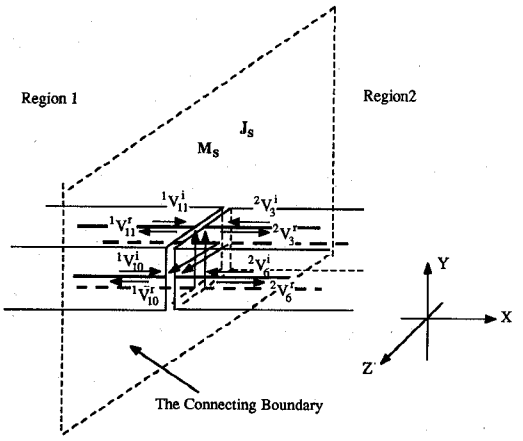

Fig. 7. Connecting boundary placed between two TLM regions.

$$\mathbf{J_s} = J_y\mathbf{a_y} + J_z\mathbf{a_z}, \tag{26}$$

and introducing the equivalence between FD–TD and TLM described in [18], one obtains

$$-M_y = E_{z1} - E_{z2} \equiv \left({}^1V^r_{10} + {}^1V^i_{10}\right) - \left({}^2V^r_6 + {}^2V^i_6\right) \tag{27}$$

$$-J_z = H_{y1} - H_{y2} \equiv \left({}^1V^r_{10} - {}^1V^i_{10}\right)/Z_0 - \left({}^2V^i_6 - {}^2V^r_6\right)/Z_0, \tag{28}$$

and

$$M_z = E_{y1} - E_{y2} \equiv \left({}^1V^r_{11} + {}^1V^r_{11}\right) - \left({}^2V^r_3 + {}^2V^i_3\right) \tag{29}$$

$$J_y = H_{z1} - H_{z2} \equiv \left({}^1V^i_{11} - {}^1V^r_{11}\right)/Z_0 - \left({}^2V^r_3 - {}^2V^i_3\right)/Z_0, \tag{30}$$

which lead to the connecting boundary conditions:

$${}^1V^r_{10} = -\frac{1}{2}(M_y + Z_0J_z) + {}^2V^i_6 \tag{31}$$

$${}^2V^r_6 = \frac{1}{2}(M_y - Z_0J_z) + {}^1V^i_{10} \tag{32}$$

$${}^1V^r_{11} = \frac{1}{2}(M_z - Z_0J_y) + {}^2V^i_3 \tag{33}$$

$${}^2V^r_3 = -\frac{1}{2}(M_z + Z_0J_y) + {}^1V^i_{11} \tag{34}$$

where ${}^1V^i_{10}$, ${}^1V^r_{10}$, ${}^1V^i_{11}$, ${}^1V^r_{11}$, ${}^2V^i_6$, ${}^2V^r_6$, ${}^2V^i_3$, and ${}^2V^r_3$ are the impulses incident and reflected at the interface between regions 1 and 2, as shown in Fig. 7. The current source components are computed by (23) and (24). The preceding equations hold for arbitrary excitations (which are usually expressed analytically). To reduce the numerical noise generated by the TLM model in the presence of absorbing boundaries, it is necessary to use low-frequency excitations for the incident fields because they are usually analytically computed and then introduced at connecting boundaries as equivalent currents. Consequently, they always travel at a constant velocity (velocity of light) regardless of their frequency. However, scattered fields, which are evaluated numerically, travel at lower velocity at higher frequencies due to the numerical dispersion of the TLM model. As a result, incident and scattered fields do not generally reach a given location in synchronism, and, consequently, errors are generated. For instance, scattered fields are supposed to reach a shadow region at the same time as incident waves to yield an almost zero field region. However, this may not happen in numerical simulations due to the delay undergone by scattered-wave high-frequency components.

V. Validations of Absorbing and Connecting Boundary Conditions for TLM Simulations

An appropriate way to validate numerical time-domain techniques is to discuss results in the frequency domain rather than in the time domain. The reason is that numerical models exhibit some severe dispersion (in both space and velocity) in the high-frequency range due to their finite discretization scheme. Consequently, incorrect results may be generated preponderently for high-frequency components, which may not be evaluated easily for comparison in the time domain. Conversely, all the models tend to be correct for low-frequency modeling. This also applies to validations of models including different schemes interfaced. Thus, validations of absorbing boundary conditions for the TLM model are performed in the frequency domain, and for relatively low frequencies, rather than in the time domain.

A. Computations of Reflections of Absorbing Boundaries in Rectangular Waveguides

Consider a section of the WR28 rectangular waveguide in which the waves can be considered as a superposition of many plane waves bouncing back and forth on the walls at different incident angles. Therefore, behavior of the wide-angle absorption of the absorbing boundaries can be evaluated. Simulations were performed using a 2D-TLM shunt node network and 3D-TLM SCN network, respectively. Both ends of the waveguide were terminated with the absorbing boundaries. The Voltage Standing-Wave Ratio (VSWR) in the waveguide is computed directly and numerically with the ratio of $V_{\max}$ over $V_{\min}$, where V is the amplitude of the dominant mode in the waveguide. Fig. 8 shows the return losses in the simulations which are more than -35 dB over a wide range of frequencies has been achieved for both 2D and 3D cases. It can also be observed that Taylor's series expansion technique displays slightly better performance than Higdon's approach in the high-frequency range, whereas the trend is reversed at lower frequencies. Knowing that near cutoff the dominant mode strikes the absorbing walls at grazing angles, one can conclude that Higdon's approach yields a better performance under this situation. This conclusion is corroborated by results shown in Figs. 1 and 5.

B. Validations of Absorbing and Connecting Boundary Conditions with Scattering Problems

1) Two Dimensions: Fig. 9 illustrates a 0.1-wavelength-thick conducting screen that extends 0.5 wavelength to each side of a straight slot having a gap of 0.025 wavelength. Broadside Transverse (TE) illumination is assumed. Two types of predictive data are compared: 1) the high-resolution $(0.025\lambda_0)$

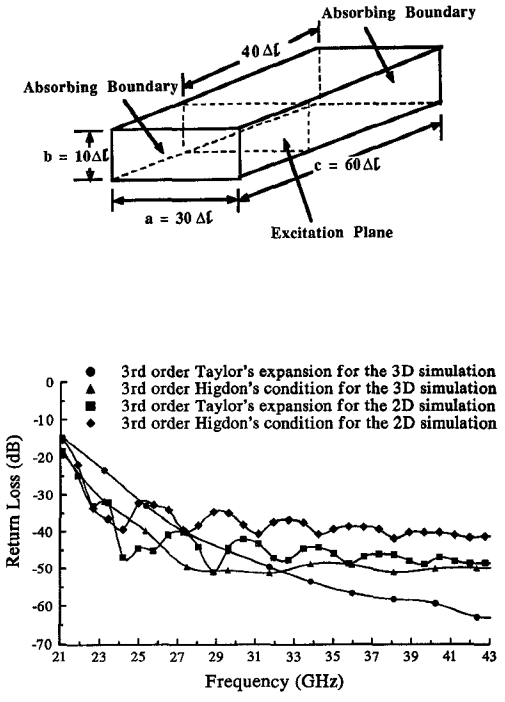

Fig. 8. Return loss in rectangular waveguide with TLM simulations.

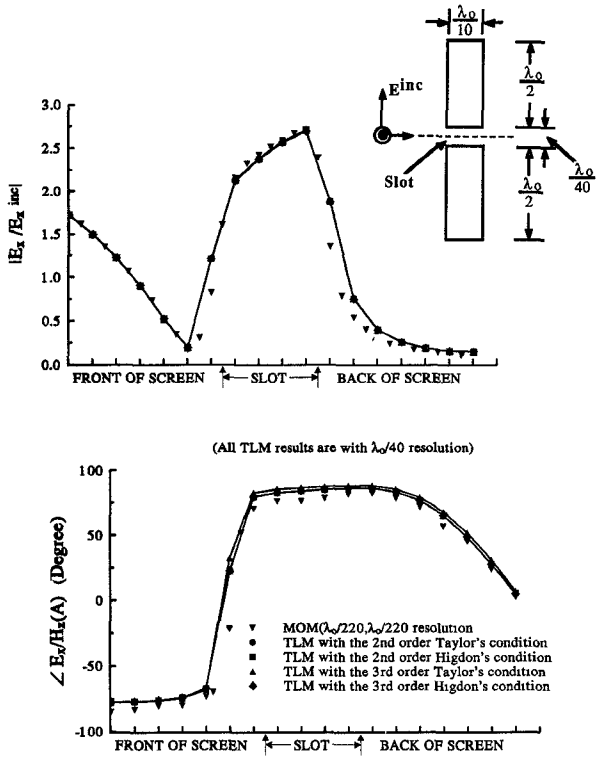

Fig. 9. Comparison of TLM and frequency-domain surface EFIE results for gap electric field distribution in slotted screen.

TLM model treating the slot as a one-cell gap (absorbing boundaries are placed uniformly 15 cells away from the conducting sheet); 2) a very high resolution frequency-domain EFIE model, solved via Moment Method (MOM) (having $0.0025\lambda_0$ sampling in the slot), which treats the slotted screen as a pure scattering geometry [21]. From Fig. 9 one can see that there is good agreement between the two sets of results in both magnitude and phase.

2) Three Dimensions: Consider a metal cube (Fig. 10) with electrical size $k_0 s = 2$, where s is the side width of the cube, subject to plane-wave illumination at broadside incidence. Results shown in Fig. 10 are for the TLM (SCN) simulation and a frequency-domain surface EFIE using a standard triangular surface-patching MOM code [17]. For the TLM model, each face of the cube is spanned by 144 square cells (12×12), and the absorbing boundary is again located at a uniform distance of 15 cells from the cube surface. For the MOM model, each face of the cube is spanned by 32 triangular patches. Comparative results are shown for the surface current along path $\overline{abcd}$, which is the plane of the incident electric field (see Fig. 10). The surface currents were obtained from the expression $\mathbf{n} \times \mathbf{H}$ on the metal surface, where $\mathbf{H}$ is obtained from the currents in the TLM network [18] and $\mathbf{n}$ is the outward normal unit vector. A very high degree of correspondence exists between the two sets of results, which again shows the good performance of the absorbing and connecting boundary conditions presented herein.

The simulation results do not show the case for which simple matched load termination was used for limiting the TLM network. In fact, this simple technique yields acceptable results only when such terminations are located in regions where a simple radiation condition prevails. This is obviously not the case in the preceding examples for which the advantage of more complicated absorbing boundary conditions is demonstrated in the relatively near field. Comparisons that show the better performance of higher order absorbing conditions versus the simple matching approach can be seen in [6] and [8], for the 2D and 3D cases respectively.

In terms of computer expenditures, the addition of algorithms that process fields at absorbing and connecting boundaries requires about the same CPU time as for FD–TD. However, it was shown [18] that if TLM requires a slightly larger computer cost than FD–TD (Yee's scheme) in terms of the basic algorithm, this is largely compensated by a faster convergence for the TLM model. Finally, comparison in terms of computer cost with MOM is difficult because it is a frequency-domain approach. It is clear that for single-frequency characterization, it has a great advantage over time-domain methods. Conversely, wide frequency band analyses *via* fast Fourier transform time-domain techniques are far more efficient and have no analytical preprocessing.

3) Instabilities of Absorbing Boundaries: Numerical experience has shown that unstable solutions may still occur due to the following reasons.

a) Absorbing boundaries too close to the source: Since most of absorbing conditions are derived under the assumption that waves are traveling or propagating, they may amplify, instead of "absorbing" evanescent waves that are usually present in regions near sources and discontinuities. It is suggested that the absorbing boundaries be placed at 10–15 cells from sources and discontinuities in both 2D- and 3D-TLM simulations.

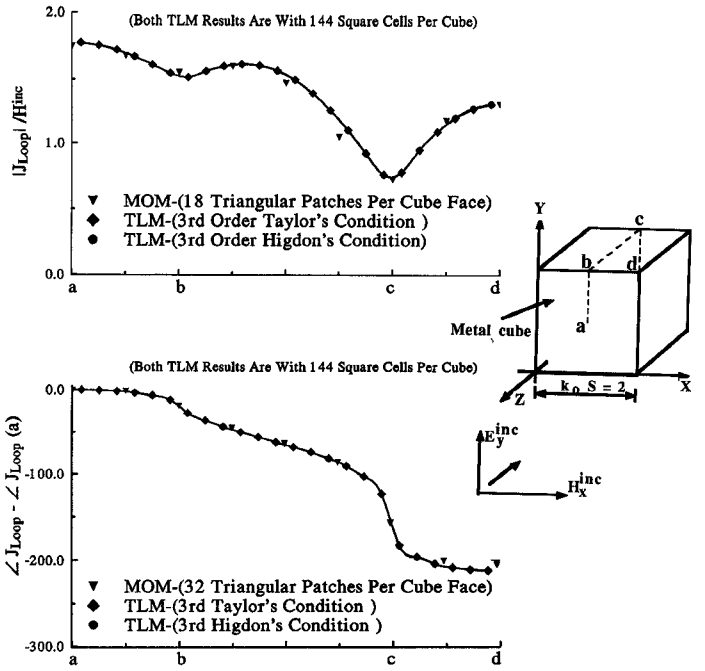

Fig. 10. Comparison of TLM and MOM results for surface currents on the metal cube.

b) Numerical noises: Truncation errors that occur in computer simulations produce uncorrelated noise, which becomes the predominant signal component in computation domains after the major part of the electromagnetic energy response has passed through the absorbing boundaries. Since most of the absorbing boundary conditions are derived on the basis of physical correlated wave propagation, instabilities may occur when numerical noise becomes the predominant component of the signal processed at the boundaries as described in [23]. To overcome or delay the occurrence of instabilities, two techniques were employed herein: 1) use a frequency-band-limited excitation, which reduces the high temporal frequency components in the simulations; 2) switch to other boundary conditions such as lossy boundary conditions after the major part of the energy response has passed the absorbing boundaries.

c) Orders of absorbing boundaries too high: Since TLM models are second (or slightly higher)-order finite-difference operations higher orders which are required for higher order absorbing boundaries cannot be computed correctly by TLM models, leading to unstable solutions. From experience, it is recommended that up to the fifth order of absorbing boundaries be applied for the 2D-TLM simulations, and the third order for the 3D-TLM simulations.

VI. Conclusion

In this paper, the absorbing boundary and connecting boundary conditions have been studied and developed for two and three-dimensional transmission-line matrix (TLM) simulations. The performance of two absorbing boundary conditions based on Higdon's and Taylor's expansion algorithms were examined and validations of both absorbing and connecting boundaries were obtained in the two- and three-dimensional cases. For instance, an excellent level of return loss was achieved over a wide frequency range for matched load simulations pertaining to the dominant mode of a rectangular waveguide. In addition, good agreement between TLM simulation results and MOM solutions was found in the case of three-dimensional scattering problems.

It was observed that the second- and third-order absorbing boundary conditions are sufficient to achieve negligible levels of reflection and that higher orders do not improve the accuracy of solutions.

References

[1] P. B. Johns and R. L. Beurle, "Numerical solution of 2-dimensional scattering problems using a transmission-line matrix," *Proc. Inst. Elec. Eng.*, vol. 118, no. 9, pp. 1203–1208, 1971.

[2] W. J. R. Hoefer, "The transmission line matrix (TLM) method," in *Numerical Techniques for Passive Microwave and Millimeter-Wave Structures*, T. Itoh, Ed. New York: Wiley, 1989, chap. 8, pp. 486–591.

[3] ——, "Time domain electromagnetic simulation for microwave CAD application," *IEEE Trans. Microwave Theory Tech.*, vol. MTT-40, pp. 1517–1527, 1992.

[4] Eswarappa, G. I. Costache, and W. J. R. Hoefer, "TLM modelling of dispersive wide-band absorbing boundaries with time domain diakoptics for S-parameters extraction," *IEEE Trans. Microwave Theory Tech.*, vol. MTT-38, pp. 379–386, 1990.

[5] N. R. S. Simons and E. Bridges, "Method for modelling free space boundaries in TLM simulations," *Electronics Lett.*, vol. 26, no. 7, pp. 453–455, Mar., 1990.

[6] ——, "Application of the TLM method to two-dimensional scattering problems," *Int. J. Num. Modelling: Electron. Network, Devices, Fields*, vol. 5, pp. 93–119, 1992.

[7] P. Saguet, "TLM method for the three dimensional analysis of microwave and mm-wave structures." Paper presented at Int. Workshop of the German IEEE MTT/AP Chapter on CAD Oriented Numerical Techniques for the Analysis of Microwave and MM-Wave Transmission-Line Discontinuities and Junctions, Stuttgart, Germany, Sept. 13, 1991.

[8] J. A. Morente, J. A. Porte, and M. Khalladi, "Absorbing boundary conditions for the TLM method," *IEEE Trans. Microwave Theory Tech.*, vol. MTT-40, no. 11, pp. 2095–2099, 1992.

[9] Z. Liao, L. Wong, B. Yang, and Y. Yuan, "A transmitting boundary for transient wave analysis," *Scientia Sinica (Series A)*, vol. XXVII, pp. 1062–1076, Oct. 1984.

[10] R. L. Higdon, "Numerical absorbing boundary conditions for the wave equation," *Math. Comp.*, vol. 49, no. 179, pp. 65–91, 1987.
[11] E. L. Lindman, "Free-space' boundary conditions for the time dependent wave equations," *J. Comput. Phys.*, vol. 18, pp. 66–78, 1975.
[12] J. G. Blaschak and G. A. Kriegsmann, "A comparative study of absorbing boundary conditions," *J. Comput. Phys.*, vol. 77, pp. 109–139, 1988.
[13] J. Fang, "Time-domain finite-difference computation for Maxwell's equations," Ph.D. Dissertation, University of California, Berkeley, 1989.
[14] T. G. Moore, J. G. Blashchak, A. Taflove, and G. A. Kriegsmann, "Theory and application of radiation boundary operators," *IEEE Trans. Antennas Prop.*, vol. AP-36, no. 12, pp. 1797–1811, 1988.
[15] W. Railton and C. Daniel, "Comparison of the effect of discretization on absorbing boundary algorithms in the finite difference time domain method," *Electron. Lett.*, vol. 28, no. 20, pp. 1891–1893, Sept. 1992.
[16] K. Umashankar and A. Taflove, "A novel method to analyze electromagnetic scattering of complex objects," *IEEE Trans. Electromag. Compat.*, vol. EMC-24, pp. 397–405, 1982.
[17] A. Taflove and K. Umashankar, "Radar cross section of general three-dimensional scatterers," *IEEE Trans. Electromag. Compat.*, vol. EMC-25, no. 4, pp. 433–440, 1983.
[18] Z. Chen, M. M. Ney, and W. J. R. Hoefer, "A new finite-difference time-domain formulation and its equivalence with the TLM symmetrical condensed node," *IEEE Trans. Microwave Theory Tech.*, vol. MTT-39, pp. 2160–2169, 1991.
[19] L. Halpern, "Wide-angle one-way equations," *J. Acoust. Soc. Am.*, vol. 84, no. 4, pp. 1397–1404, Oct. 1988.
[20] J. Nielsen "Spurious modes of the TLM-condensed node formulation," *IEEE Trans. Microwave Guided Wave Lett.*, vol. 1, pp. 201–203, 1991.
[21] A. Taflove, K. Umashankar, B. Beker, F. Harfoush, and Y. S. Yee, "Detailed FD–TD analysis of electromagnetic fields penetrating narrow slots and lapped joints in thick conducting screens," *IEEE Trans. Antennas Propag.*, vol. AP-36, pp. 247–257, 1988.
[22] R. F. Harrington, *Time-Harmonic Electromagnetic Fields*. New York: McGraw-Hill, 1961.
[23] J. Fang, "Investigation on the stability of absorbing boundary conditions for the time-domain finite-difference method," in *1992 IEEE Antennas Propagat. Int. Symp. Digest*, Chicago, July 1992, pp. 548–551.

Zhizhang Chen (SM'92) was born in Fujian, People's Republic of China. He obtained the B.Eng. degree in radio engineering from Fuzhou University, People's Republic of China, in 1982, the M.Eng. degree in electrical engineering from Southeast University, Nanjing, People's Republic of China, in 1985, and the Ph.D. degree from the University of Ottawa, Canada, in 1992.

From 1985 to 1988, he was with the Department of Radio Engineering, Fuzhou University, where he became a Lecturer in 1987. After three years of teaching courses in microwaves and doing research on communications systems, he joined the Department of Electrical Engineering, University of Ottawa, and pursued the Ph.D. degree. Currently, he is a Postdoctoral Fellow with the same department. His research interests include microwave measurement techniques, computer-aided design of high-frequency circuits and devices, and numerical techniques for modeling and simulation of electromagnetic fields.

Michel M. Ney (SM'91) received the Engineer Diploma from the Swiss Federal Institute of Technology of Lausanne, Switzerland, in 1976, and the Ph.D. degree from the University of Ottawa in 1983.

Since 1983 he has been with the Laboratory for electromagnetics and Microwaves of the Department of Electrical Engineering at the University of Ottawa, where he is presently Professor. He spent his sabbatical leave in 1991 at the Swiss Federal Institute of Technology in Lausanne as a Visiting Professor with the Electromagnetic and Acoustic Laboratory. His research interests include passive millimeter-wave circuit design, electromagnetic engineering, electromagnetic interference and compatibility problems, and numerical modeling.

Dr. Ney is a Registered Professional Engineer in the province of Ontario, Canada.

Wolfgang J. R. Hoefer (F'91) received the Dipl.-Ing. degree in electrical engineering from the Technische Hochschule, Aachen, Germany, in 1965, and the D.Ing. degree from the University of Grenoble, France, in 1968.

During the academic year 1968/69 he was a Lecturer at the Institut Universitaire de Technologie de Grenoble and a Research Fellow at the Institut National Polytechnique de Grenoble, France. In 1969 he joined the Department of Electrical Engineering at the University of Ottawa, Canada, where he was a Professor until March 1992. Since April 1992 he has been the NSERC/MPR Teltech Industrial Research Chair in RF engineering in the Department of Electrical and Computer Engineering, the University of Victoria, Canada, and he is a Fellow of the Advanced Systems Institute of British Columbia. During sabbatical leaves he spent six months with the Space Division of AEG-Telefunken in Backnang, Germany (now ATN), and six months with the Electromagnetics Laboratory of the Institut National Polytechnique de Grenoble, France, in 1976/77. During 1984/85 he was a Visiting Scientist at the Space Electronics Directorate of the Communications Research Centre in Ottawa, Canada. He spent a third sabbatical year in 1990/91 as a Visiting Professor at the University of Rome "Tor Vergata" in Italy, the University of Nice–Sophia Antipolis in France, and the Technical University of Munich in Germany. His research interests include numerical techniques for modeling electromagnetic fields and waves, computer-aided design of microwave and millimeter-wave circuits, microwave measurement techniques, and engineering education.

He is the Co-founder and Managing Editor of the International Journal of Numerical Modelling.